Channeling Studies in Diamond-Type Lattices

S. T. PICRAUX,* J. A. DAVIES, L. ERIKSSON,† N. G. E. JOHANSSON,† AND J. W. MAYER*
Chalk River Nuclear Laboratories, Chalk River, Ontario, Canada
(Received 25 November 1968)

The channeling characteristics of protons and helium ions in various diamond-type lattices (diamond, Si, Ge, GaP, GaAs, and GaSb) have been studied by means of Rutherford backscattering in the 0.5–2-MeV range. Critical angles ($\psi_{1/2}$) and minimum yields (χ_{min}) have been measured and compared to theory. The values of $\psi_{1/2}$ for axial channeling have a functional dependence which agrees well with calculations based on the average potential along the row—both for uniform and for nonuniform spacing and (in the case of the compound semiconductors) for mixed atomic composition. However, the measured values are $\approx 25\%$ lower in absolute magnitude. Planar critical angles show a faster attenuation with decreasing planar spacing than predicted, but in other aspects agree with theory. In the compound semiconductors, the orientation dependence of backscattering and of x-ray yields has been used to investigate simultaneously the interaction of the beam with both atomic species in the lattice. For those directions along which the different atomic species lie on separate rows (e.g., ⟨110⟩), each row steers the incident particles in a manner described by the average potential of that row.

I. INTRODUCTION

IN recent years, much effort has been spent in studying the motion of energetic charged particles in single crystals. Whenever a low-index crystal axis or plane is aligned with a beam of positively charged particles, one observes a significant reduction in energy loss and an even larger reduction in the yield of processes requiring a close encounter with the lattice atoms (such as Rutherford backscattering, nuclear reactions, and inner shell x-ray production). The interest in this "channeling" effect lies both in the further understanding of the channeling mechanism itself and in its application to the study of the solid state.

Among the various applications of channeling as an analytical tool have been foreign atom location,[1,2] lattice disorder,[3] surface effects,[4] and nuclear lifetimes.[5] One particularly fruitful application has been the study of ion implantation in semiconductors[6] in which the location of the implanted ions and a determination of the damage produced in the lattice is studied by means of the channeling behavior of MeV-projectiles.

In the study of channeling itself, the diamond-type lattice is a particularly interesting structure. Within a given crystal, one may select a direction where the steering of the channeled particles is due either to a row of uniformly spaced atoms (such as the ⟨110⟩, Fig. 1), or to a nonuniformly spaced row (⟨111⟩). Furthermore, in a compound crystal such as GaP, one has, along the ⟨110⟩ [Fig. 2(a)], separate monatomic rows of Ga and P, whereas along the [111] direction all rows contain both Ga and P. In addition, because of the asymmetric spacing along the ⟨111⟩, the ⟨111⟩ and ⟨$\bar{1}\bar{1}\bar{1}$⟩ configurations are not equivalent. Similar variations may be found for certain planar configurations [Fig. 2(b)]: The interplanar spacing is uniform for the {110} and nonuniform for the {111}; in compound crystals, individual planes also may or may not contain both types of atoms [Fig. 2(b)].

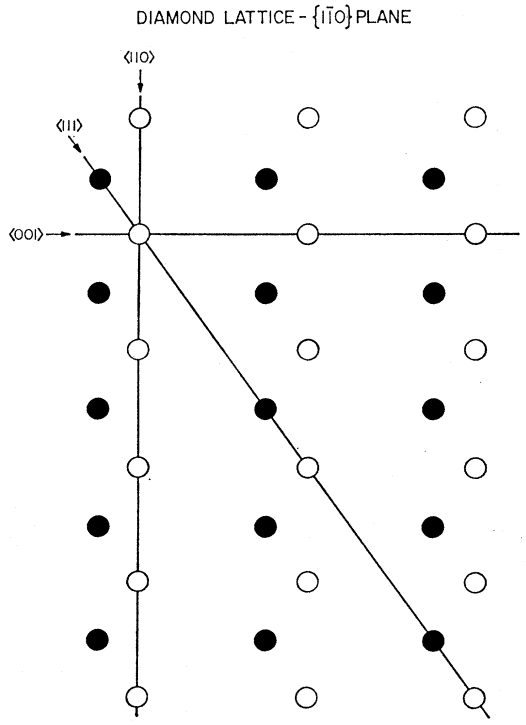

FIG. 1. Atomic positions in the (1$\bar{1}$0) plane of the diamond-lattice structure showing the three major axial directions ⟨110⟩, ⟨111⟩, and ⟨001⟩. The solid and open circles distinguish between the two different types of atoms for a diatomic lattice such as GaP.

* Permanent address: California Institute of Technology, Pasadena, Calif. Supported in part by USAF Cambridge Research Laboratory.
† Permanent address: Research Institute for Physics, Stockholm 50, Sweden.
[1] E. Bøgh, in *Interaction of Radiation with Solids*, edited by A. Bishay (Plenum Press, Inc., New York, 1967), p. 361.
[2] L. Eriksson, J. A. Davies, J. Denhartog, Hj. Matzke, and J. L. Whitton, Can. Nucl. Tech. **5**, 40 (1966).
[3] J. W. Mayer, L. Eriksson, S. T. Picraux, and J. A. Davies, Can. J. Phys. **46**, 663 (1968).
[4] E. Bøgh, Can. J. Phys. **46**, 653 (1968).
[5] F. Brown, D. A. Marsden, and R. D. Werner, Phys. Rev. Letters **20**, 1449 (1968).
[6] L. Eriksson, J. A. Davies, N. G. E. Johansson, and J. W. Mayer, J. Appl. Phys. **40**, 842 (1969).

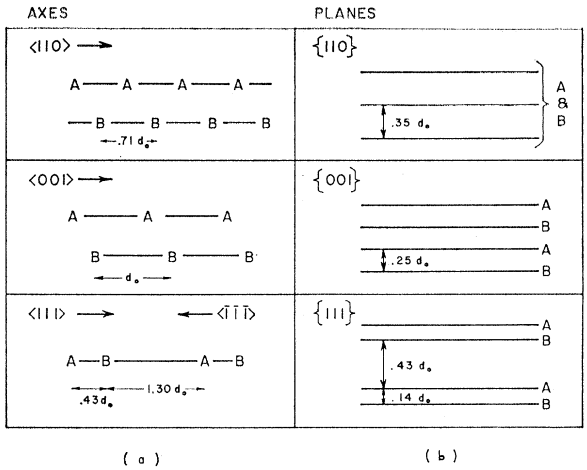

FIG. 2. Spacing of atoms along axial directions (a) and between planes (b) for the diatomic diamond-type lattice with atoms A and B and lattice constant d_0. For monoatomic lattices A=B.

The influence of different lattice spacing or composition is most directly seen in measurements of the critical angle, the minimum yield, and the energy loss for channeled particles. Previous channeling measurements have been made in the monatomic diamond lattices of Si and Ge by Appleton *et al.*[7] and Davies *et al.*[8] Channeled particle energy-loss measurements have been made in these materials and in GaAs by Sattler *et al.*[9] Recent measurements by Eriksson *et al.*[10] with UO_2, another type of compound lattice, indicate that atomic composition has a large effect on critical angles and values of the minimum yield, and particularly on their depth dependence.

The main purpose of this paper is to compare the channeling behavior observed in various diamond-type lattices to theory.[11,12] Our results show that the values of the axial critical angles for different projectiles, energies, and semiconductor targets have a functional dependence that is consistent with the use of average potentials. In general, we have used wide-angle Rutherford scattering to investigate critical channeling angles. The advantage of Rutherford scattering is that good depth resolution is possible, and so the critical angle can be measured simultaneously at several depths within the first μ of the surface. This enables the effects of dechanneling to be investigated and a suitable correction applied, if necessary.

As shown by Khan *et al.*,[13] x-ray production may also be used to measure the critical angle. The advantage of x rays lies in the ability to study independently the interaction of the beam with each atomic species of a compound lattice. By utilizing the difference in energies of the characteristic x rays, it has been possible in GaSb, for example, to measure the critical angles for both the Ga and the Sb sublattices, simultaneously.

Projectile energies of 500 keV–2 MeV were used, since this was the energy range employed in most of the applications. A few measurements in silicon at energies of 50 keV have also been made because, in ion implantation (typically in the 20–100 keV range), it is often desirable to orient the crystals by a proton beam at these energies before implantation. This preorientation can be quite important in implantation studies when one considers that, because of differences in the amount of electronic and nuclear stopping, both ion ranges (Eriksson *et al.*)[14] and lattice disorder (Nelson *et al.*)[15] are strongly influenced by channeling behavior.

II. EXPERIMENTAL

The measurements were carried out on the Chalk River 2-MeV Van de Graaff using a technique similar to that in previous work. For more details of the experimental arrangement see, for example, Davies *et al.*[8] The goniometer rotation (ϕ) and tilt (θ) angles could be set reproducibly to 0.02°. An additional adjustment on the crystal holder made it possible to tilt the crystal until its axis coincided with the rotation axis (ϕ) of the goniometer. This simplified the measurement of axial critical angles.

A monoenergetic beam of protons or helium ions was used. Typical currents were 2 nA and the beam divergence was less than 0.05°. The backscattered particles were measured with a surface barrier detector placed about 5 cm from the crystal (Fig. 3). The scattering angle was 160° and the angle subtended by the detector

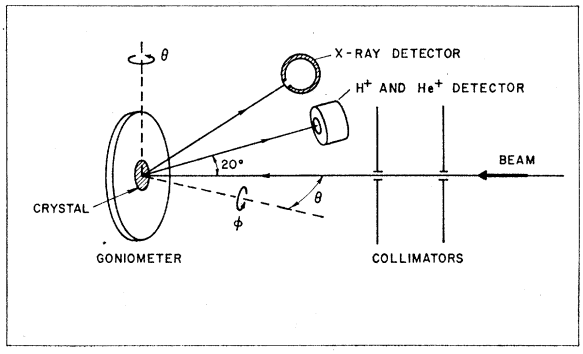

FIG. 3. Schematic diagram of the experimental arrangement.

[7] B. R. Appleton, C. Erginsoy, and W. M. Gibson, Phys. Rev. **161**, 330 (1967).
[8] J. A. Davies, J. Denhartog, and J. L. Whitton, Phys. Rev. **165**, 345 (1967).
[9] A. R. Sattler and G. Dearnaley, Phys. Rev. **161**, 244 (1967).
[10] L. Eriksson and J. A. Davies, Arkiv Fysik (to be published).
[11] J. Lindhard, Kgl. Danske Videnskab. Selskab, Mat.-Fys. Medd. **34**, 14 (1965).
[12] S. Datz, C. Erginsoy, G. Leibfried, and H. O. Lutz, Ann. Rev. Nucl. Sci. **17**, 129 (1967).
[13] J. M. Khan, D. L. Potter, and R. D. Worley, Phys. Rev. **148**, 413 (1966).
[14] L. Eriksson, J. A. Davies, and P. Jespersgaard, Phys. Rev. **161**, 219 (1967); L. Eriksson, *ibid.* **161**, 235 (1967).
[15] R. S. Nelson and D. J. Mazey, Can. J. Phys. **46**, 689 (1968).

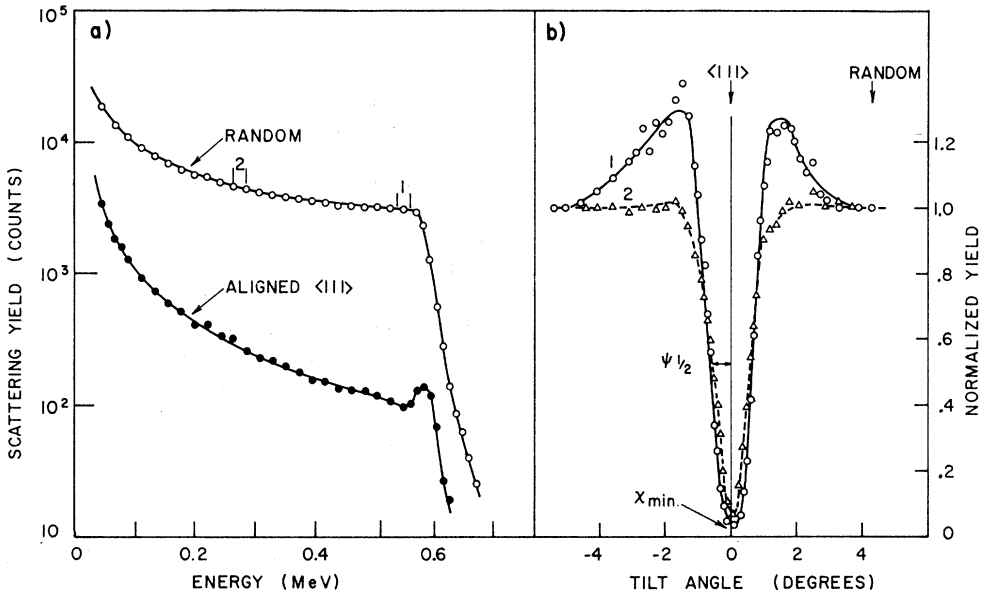

FIG. 4. (a) Energy spectra for 1-MeV helium ions backscattered from a silicon crystal: ●—beam incident along the ⟨111⟩; ○—beam incident in a "random" direction. The energy regions 1 and 2 indicate the two single-channel-analyzer settings used in 4(b). These correspond to depths of 900 and 6000 Å, respectively. (b) Orientation dependence of the normalized yield obtained from the energy regions 1 and 2 [Fig. 4(a)]. Tilt angles marked "⟨111⟩" and "random" show the orientations at which the energy spectra of Fig. 4(a) were taken.

was large (~12°) so as to reduce crystalline effects along the outgoing trajectory. Energy analysis was performed by a 100-channel analyzer and by 8 single-channel analyzers with scalers. The energy resolution of the solid-state detector was approximately 20-keV full width at half maximum (FWHM) for 1-MeV helium ions.

The characteristic x-ray yields could be measured simultaneously, using a gas-filled proportional counter similar to the type described by Khan.[13] For these measurements, helium-ion scattering was used in order to confine x-ray production to a region near the surface.[16] A Mylar window 14.5 μ thick prevented the scattered helium ions from entering the detector.

Typical energy spectra of the backscattered particles are shown in Fig. 4(a). The random spectrum is obtained by orienting the crystal so that the incident beam is not aligned with any crystal axis or plane. The aligned spectrum shows the large reduction in backscattered yield when a crystal axis (⟨111⟩ in this case) is parallel to the beam direction. The particles with highest energy (i.e., at the spectrum edge) correspond to scattering off the surface of the crystal. The helium ions lose energy as they move through the crystal, so that the continuum at lower energies corresponds to scattering from progressively larger depths. Detailed orientation scans from two different depths in silicon are shown in Fig. 4(b). These are obtained by recording the yield in the narrow energy regions 1 and 2 [Fig. 4(a)] while tilting the ⟨111⟩ axis through the beam direction. The critical angle is determined by measuring the angular half-width ($\psi_{1/2}$) at a level midway between the aligned and random levels. The accuracy of the axial critical-angle measurements is estimated to be ±0.06°.

The observed critical angle ($\psi_{1/2}$) and minimum yield (χ_{min}) both depend on the depth beneath the surface at which the measurements are made. The minimum yield χ_{min} is defined as the ratio of the yield in the perfectly aligned direction to that in a random direction. It is therefore a direct measure of the unchanneled fraction of the beam. Its depth dependence can be obtained from the aligned and random spectra of Fig. 4(a). From the results in Fig. 5, it can be seen that, even at a depth of 6000 Å, more than 90% of the beam is still channeled. Germanium shows a significantly larger dechanneling rate than silicon—as one might expect, since it has a larger vibrational amplitude.

The variation of critical angle with depth is illustrated in Figs. 4(b) and 6. In the case of silicon, we see very little difference between the ⟨111⟩ critical angle for 1-MeV helium ions at 900 and 6000 Å [Fig. 4(b)]. On the other hand, in germanium a significant variation is observed over the same depth region (Fig. 6); in this case, the angles are measured simultaneously at several depths over the region 500–8000 Å, and extrapolation to the surface is then made to allow comparison with theory. Figure 6 also demonstrates the increased importance of depth effects at lower projectile energies in

[16] J. A. Davies, L. Eriksson, N. G. E. Johansson, and I. V. Mitchell, Phys. Rev. (to be published).

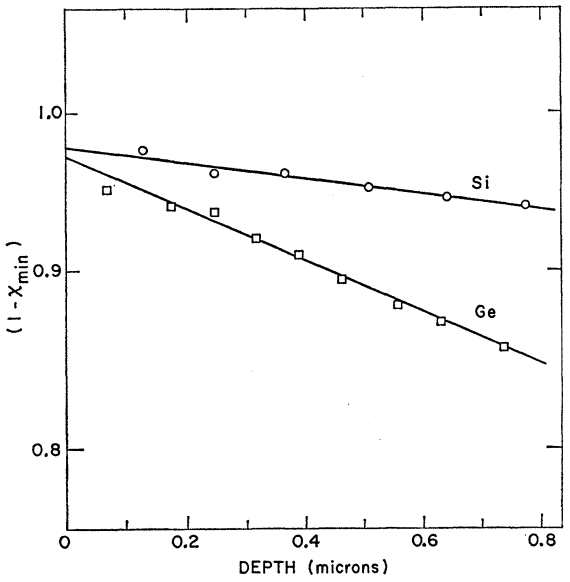

FIG. 5. Depth dependence of χ_{min} for 1-MeV helium ions along the ⟨111⟩ axis in silicon and germanium.

the axial case. For planar channeling, on the other hand, the depth dependence of $\psi_{1/2}$ is seen to be rather small and is relatively insensitive to energy variations.

In measuring planar and axial critical angles, care must be taken to avoid competing effects from higher-order directions or planes. Figure 7 indicates the complexity that exists (see also Fig. 5 in Ref. 8). Indeed, it is often difficult to find a truly random plane (or tilt angle) in which to tilt (or rotate) the crystal.

III. THEORY

The value of $\psi_{1/2}$ has been treated in Lindhard's theory on directional effects.[11] The critical angle for axial channeling is predicted to be

$$\psi_{1/2}=\alpha\psi_1, \tag{1}$$

where ψ_1 is a characteristic angle expressing the functional dependence on energy, atomic number, and lattice spacing, and α is a *constant* depending only on the vibrational amplitude of the lattice atoms. Calculations by Andersen[17] show that typical values of α range from 0.8 to 1.6.

In Lindhard's treatment, the axial rows of atoms that steer the channeled particles are treated in terms of the average potential of the row or "string" of atoms, and the characteristic angle is determined from the maximum transverse energy for which a particle may still be steered. For a monatomic row of atoms with uniform spacing the result obtained is

$$\psi_1=(2Z_1Z_2e^2/Ed)^{1/2}, \text{ provided}[18]\ \psi_1\lesssim a/d, \tag{2}$$

where Z_1 and Z_2 are the atomic numbers of the projectile and target atoms, respectively, e the electronic charge, a the Thomas-Fermi screening distance, d the lattice spacing along the row, and E the projectile energy.

For the case of more than one type of atom along the rows or for nonuniform spacing of the atoms, use of an averaged potential calculation gives

$$\psi_1=(2Z_1\bar{Z}_2e^2/E\bar{d})^{1/2}, \text{ again provided } \psi_1\lesssim a/\bar{d}, \tag{3}$$

where $\bar{Z}_2$ is the average atomic number of the atoms along the row and $\bar{d}$ is their average spacing.

The planes may be treated in a similar but less quantitative manner. Using an averaged sheet potential for the case of uniformly spaced planes leads to a planar critical angle

$$\psi_{1/2}=\beta(Z_1Z_2e^2Nd_pa/E)^{1/2}, \tag{4}$$

where N is the atomic density, d_p is the spacing between planes, and the factor β is of the order of unity. The proportionality constant β for planar channeling is expected to be only mildly temperature-dependent.

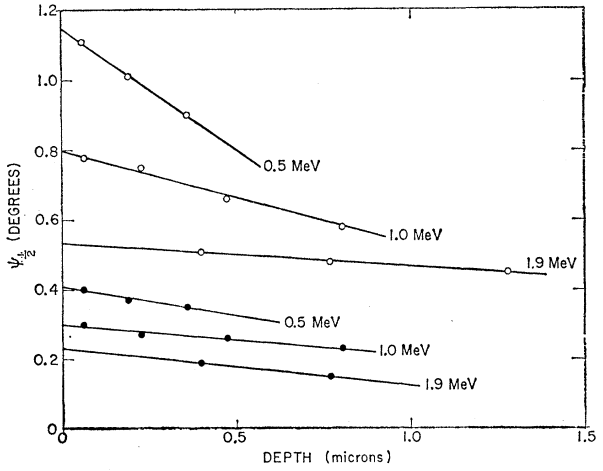

FIG. 6. Depth dependence of $\psi_{1/2}$ for the ⟨111⟩ axis (○) and the (110) plane (●) in germanium, using 0.5-, 1.0-, and 1.9-MeV He ions.

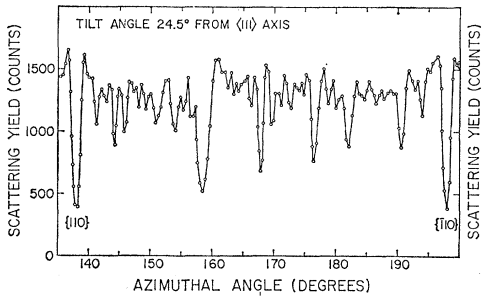

FIG. 7. Planar channeling of 1.0-MeV helium ions in germanium, measured by rotating around the ⟨111⟩ axis at a tilt angle of 24.5°.

[17] J. U. Andersen, Kgl. Danske Videnskab. Selskab, Mat.-Fys. Medd. 36, 7 (1967).

[18] This condition is fulfilled for all the data presented here (except the 50-keV H^+ in Si data).

TABLE I. Critical angles[a] in diamond-type lattices.

Crystal	Z_1	E (MeV)	$\psi_{1/2}$ axial ⟨111⟩	⟨110⟩	$\psi_{1/2}$ planar (110)	(111)	(001)	(112)	(113)
Si	H^+	0.05	3.0	3.0	0.8	0.9	0.7		
		0.25		1.02	0.32	0.33	0.25	0.20	0.16
$\alpha=1.12_5$		0.50		0.68	0.24	0.26	0.17	0.16	0.13
		1.00		0.53	0.16	0.20	0.12	0.11	0.10
		2.00		0.36	0.12	0.13	0.08	0.08	0.08
	He^+	0.50	0.98	1.10	0.30	0.32	0.23	0.19	0.16
		1.00	0.69	0.75	0.22	0.26	0.18	0.13	0.16
		2.00	0.46	0.55	0.17	0.16	0.13	0.09	0.09
Ge	He^+	0.50	1.13		0.40				
		1.00	0.80	0.95	0.30	0.23	0.18	0.20	
$\alpha=1.00$		1.90	0.54		0.23				
C (diamond)	H^+	1.00	0.46	0.54	0.16				
$\alpha=1.44$	He^+	1.00	0.58	0.75					
GaAs	He^+	0.50	1.07		0.33				
$\alpha=1.00$		1.00	0.81		0.24				
		1.90	0.48		0.14				
GaP	He^+	0.50	1.03		0.38				
$\alpha=1.17$		1.00	0.74	0.99	0.25	0.26	0.18	0.18	
		1.90	0.59		0.18				
GaSb	He^+	0.50	1.16						
$\alpha=0.99$		1.00	0.88	1.10	0.28	0.25	0.17		

[a] Estimated error for axial measurements ±0.06° (for 50-keV H^+, ±0.5°). Estimated error for planar measurements ±0.03°.

In the case of a plane containing more than one type of atom, Z_2 must of course be replaced by $\bar{Z}_2$, the mean atomic number in the plane.

IV. RESULTS AND DISCUSSION

Critical angles and minimum yields have been measured in C (diamond), Si, Ge, GaAs, GaP, and GaSb for helium ions in the 0.5 to 1.9-MeV range. Some measurements have also been made using protons. The experimental results are summarized in Tables I and II. For two of the diatomic lattices GaP and GaSb, x-ray yields were also measured in order, to study independently the steering effect of the two different atomic species. These results are given in Table III.

A. Axial $\psi_{1/2}$ Values—Monatomic Lattice

First we will compare the axial critical-angle measurements for silicon with theory. A comparison of $\psi_{1/2}$ values for the ⟨110⟩ and the ⟨111⟩ directions in a given monatomic crystal enables the change from uniform to nonuniform spacing (Fig. 1) to be studied, while keeping all other parameters fixed. This is shown in Fig. 8 for measurements in silicon at energies ranging from 250 keV to 2 MeV. The predicted value for the ⟨111⟩ direction, derived from the best fit to the ⟨110⟩ data and the change in the lattice spacing, is shown using the maximum ($d_{max}=1.30d_0$), minimum ($d_{min}=0.43d_0$), and

TABLE II. χ_{min} values along the ⟨110⟩ axis (using 1-MeV H^+ or He^+ beams).

Crystal	Projectile	Rough estimates of χ_{min} $Nd\pi\langle\rho_r^2\rangle_{av}$	$Nd\pi a^2$	χ_{min} [Calc. from Eq. (7)]	χ_{min} observed
C (diamond)	H^+	0.004	0.07	0.03	0.04
	He^+	0.004	0.06	0.03	0.05
Si	He^+	0.005	0.02	0.02	0.03
Ge	He^+	0.005	0.01	0.02	0.03
GaP	He^+	0.004_5	0.01_5	0.02	0.01_5
GaAs	He^+	0.005	0.01	0.01	0.04
GaSb	He^+	0.006	0.008	0.02	0.08

TABLE III. Comparison of $\psi_{1/2}$ values[a] from backscattering and from x-ray measurements (1.0-MeV He^+).

	$\psi_{1/2}$ along ⟨111⟩ Measured value	Corrected[b] to 1100 Å	$\psi_{1/2}$ along ⟨110⟩ Measured value	Corrected[b] to 1100 Å
GaP				
1. Backscattering[c] (from Ga atoms)	0.70	0.70	0.96	0.96
2. Ga L-shell x rays	0.61	0.62 0.70[d]	0.82	0.83 0.94[d]
3. P K-shell x rays	0.65	0.69	0.71	0.77
GaSb				
1. Backscattering[c] (from Sb atoms)	0.85	0.85	1.04	1.04
2. Sb L-shell x rays	0.70	0.78	0.93	1.04
3. Ga L-shell x rays	0.73	0.73 0.83[d]	0.82	0.82 0.93[d]

[a] Estimated experimental error: ±0.06°.
[b] Using the depth dependence of $\psi_{1/2}$ determined from the backscattering measurements (Fig. 6).
[c] All backscattering values were measured at 1100 Å depth; so no depth correction is required.
[d] Values in brackets include the empirical correction of 12% arising from the extended distribution of the L-electron shell in Ga, as discussed in the text.

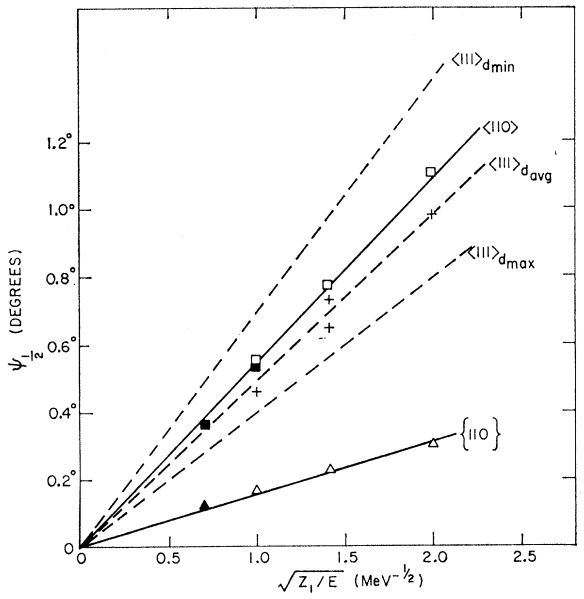

FIG. 8. The energy (E) and atomic number (Z_1) dependence of $\psi_{1/2}$ in silicon. Axial data: ⟨110⟩—□, (He^+); ■, (H^+); ⟨111⟩—+, (He^+). Planar data: {110}—△, (He^+); ▲, (H^+). Solid lines represent best fits to ⟨110⟩ and (110) data. Dashed lines are calculated for the ⟨111⟩ axis from the ⟨110⟩ data using various values for the effective lattice spacing (cf. Fig. 2 along the ⟨111⟩).

average ($d=\bar{d}=0.87d_0$) spacing along the ⟨111⟩ (Fig. 2). The experimental values (+) agree closely with the predicted curve using the average lattice spacing $\bar{d}$. Critical-angle data for the (110) plane are included in Fig. 8 to illustrate the relative magnitude for planar channeling.

The critical angles in different diamond-type lattices are compared in Fig. 9(a). Here the predicted dependence on lattice spacing, $\bar{d}$, has been removed by including a $(\bar{d})^{1/2}$ term in the abscissa. This enables both the ⟨111⟩ and ⟨110⟩ measurements to be included. A systematic deviation is observed between the diamond, silicon, and germanium data. However, as shown in Fig. 9(b), when the effect of vibrational amplitude is taken into account, using the parameter α obtained from Andersen's calculations,[17] the agreement between the three crystals is greatly improved. From Fig. 9(b) we see that the angles in germanium are only slightly lower than those in silicon and diamond. The values of α were obtained from Fig. 5 of Ref. 17, together with calculations of the rms vibrational amplitude (ρ_r) perpendicular to the axis, the lattice spacing, and the Thomas-Fermi screening distance. In the region $\rho_r/\psi_1 d>1$, a simple analytical expression for α can be given: viz., $\alpha=[\frac{1}{2}\ln(1+3a^2/\rho_r^2\ln 2)]^{1/2}$. Vibrational amplitudes were calculated from existing measurements of the Debye characteristic temperature, using the procedure outlined by Lonsdale.[19] Note that a 30% change in the value of the Debye characteristic temperature produces only a 5% change in the magnitude of α. The values of α (Table I) were constant for a given crystal within the range of critical angles measured in this study (except for 50-keV protons in Si).

Several compound semiconductors have been included in Fig. 9(b) for comparison; these are discussed further in Sec. IV B.

While all the axial critical angles measured for diamond-type lattices exhibit the predicted functional dependence on Z_1, Z_2, E, and $\bar{d}$, their average value is about 25% lower in absolute magnitude than one obtains from the theory [dotted line, Fig. 9(b)]. To remove the 25% discrepancy would require an increase in the thermal vibrational amplitude of ≈ 0.1 Å for C, Si, and Ge. This is equivalent to a value of the vibrational amplitude approximately twice that calculated from Debye temperature values. A similar discrepancy between experiment and theory has been observed in Si at somewhat higher energies,[7,8] and also in UO_2.[8,10]

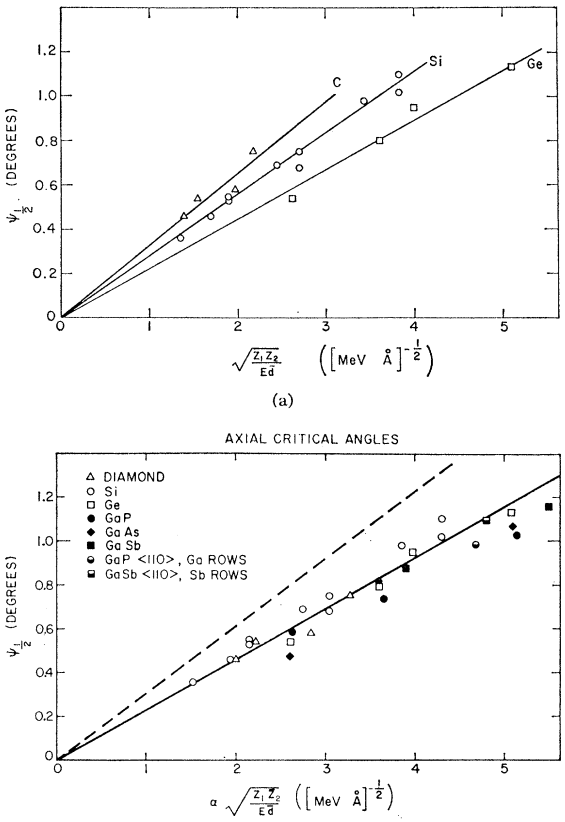

FIG. 9. (a) The observed functional dependence of axial critical angles ($\psi_{1/2}$) on energy (E), atomic number (Z_1,Z_2), and mean lattice spacing ($\bar{d}$) in various lattices: △, C (diamond); ○, Si; □, Ge. (b) As in (a), but with Andersen's calculated dependence on lattice vibrations (Ref. 17) included. Experimental data for some of the compound semiconductors are also shown. GaP, ● ⟨111⟩; ◒ ⟨110⟩ (Ga rows); GaAs, ♦ ⟨111⟩; GaSb, ■ ⟨111⟩; black and white squares ⟨110⟩ (Sb rows). The dotted line is that predicted from Eqs. (1)–(3).

[19] K. Lonsdale, Acta Cryst. 1, 142 (1948).

B. Axial $\psi_{1/2}$ Values—Diatomic Lattice

Rutherford scattering has been used to study the interaction of an incident helium-ion beam with the heavier atom of the GaP and GaSb compound crystals. We have combined such scattering studies with x-ray measurements in order to investigate simultaneously the interaction of the incident beam with both atomic species of the lattice.

1. *Rutherford Scattering Yields*

Axial critical angles measured by backscattering from the compound crystals are shown in Fig. 9(b). There are two basic cases (Fig. 2): mixed rows containing both atomic species (e.g., ⟨111⟩), and monatomic rows (e.g., ⟨110⟩ or ⟨100⟩). For a mixed row such as the ⟨111⟩, the steering of the channeled particles is due to the average effect of both types of atoms in the lattice: i.e., the critical angle is obtained using the average atomic number $\bar{Z}_2=\frac{1}{2}(Z_A+Z_B)$ and the average spacing $\bar{d}$ along the ⟨111⟩ row. The values of α (Table I) were obtained in the same manner as for the monatomic lattice, using an average value of the Thomas-Fermi screening distance in the case of the mixed rows. The agreement with the monatomic lattices and hence, with the predicted functional dependence on $\bar{Z}_2$ and $\bar{d}$ is seen to be fairly good. The GaAs angles are essentially the same as those obtained in Ge; this is not surprising since the average potential is the same as in Ge.

The ⟨111⟩ and ⟨$\bar{1}\bar{1}\bar{1}$⟩ critical angles were measured in GaP for 1-MeV helium ions. The anisotropy between these two directions is illustrated in Fig. 2. No significant difference was noted in the measured values for 1-Mev He^+. On the basis of the averaged potential theory, local anisotropy should not produce significant effects—except perhaps in the low-energy region where the continuum potential treatment is no longer applicable,[20,21] i.e., where $\psi_1 \gtrsim a/\bar{d}$. This low-energy region would correspond approximately to the energy region below 300 keV for helium in GaP.

Along the ⟨110⟩ direction, there are individual monatomic rows of the two types of atoms in the lattice (Fig. 2). Each of these rows is characterized by a critical angle within which it can steer (i.e., "channel") the incident beam. This critical angle is determined by the averaged potential of the individual row. Thus, near the surface, two separate critical angles—one corresponding to each of the two types of atomic rows—should exist. At larger depths in the crystal, the separation between the two critical angles becomes less distinct. Particles that are just within the critical angle of the Z_A row ($Z_A>Z_B$) but that have an angle greater than the critical angle of the Z_B row will undergo normal multiple scattering by close encounters with the Z_B atoms; this scattering will rapidly cause them to become dechanneled with respect the Z_A rows also.[10] This effect should not strongly influence the backscattering measurements, since distances within 1000 Å of the surface can be probed.

By backscattering from a lattice where Z_A and Z_B are not too similar, such as GaP or GaSb, the critical angle due to steering by the heavier atoms may be investigated. This is possible since the upper edge of the energy spectrum for scattering from the heavier mass atoms is greater than that for the lighter atoms. Two ⟨110⟩ $\psi_{1/2}$ values measured near the surface, corresponding to scattering from the heavier Z_A rows, have been plotted in Fig. 9(b) using $\bar{Z}_2=Z_A$. As expected, they show good agreement with the values for the monatomic lattices.

2. *X-Ray Measurements*

The x-ray yields from the two different sublattice atoms in GaP and GaSb [K-shell x rays from P (~2 keV) and the L-shell x rays from Ga (~1 keV) and Sb (~3 keV)] were monitored separately for a 1-Mev helium beam. By measuring the individual x-ray yields and backscattering yields simultaneously, it was possible to compare directly the critical angles for x-ray emission with those for backscattering from the heavier atoms (Ga in GaP and Sb in GaSb). Also the critical angles for interaction with the lighter elements were determined from the x-ray yield.

Both the x-ray and the backscattering yields should show a comparable orientation dependence, provided the mean distribution of the electron density in the shells is much less than the minimum impact parameter ($r_{\min}$) for the steering of channeled particles—as was recently demonstrated by Davies *et al.* in tungsten.[16] In the present experiment, the mean radii for the L shells of Ga and Sb and for the K shell of P are 0.10, 0.06, and 0.05 Å, respectively.[22] These are all smaller than the corresponding $r_{\min}$ values, since $r_{\min}$ is approximately given by the Thomas-Fermi screening distance a ($a_{Ga}=0.14$ Å, $a_{Sb}=0.12$ Å, $a_P=0.17$ Å). In the case of the Ga L shell, however, the difference between the mean L-shell radius and a is not very large.

Since the critical angle depends markedly on the depth beneath the crystal surface at which the yield is measured, it is necessary that the comparison between the different processes be made at similar depths. The depth from which the observed x rays originate is determined by the energy dependence of the x-ray yield and by the mass absorption coefficient. We estimate that the mean depths of the detected x rays were: Ga, 1600 Å and P, 4500 Å in GaP; Ga, 1100 Å and Sb, 3500 Å in GaSb. The corresponding depths from which

[20] The transition from the continuum (ψ_1) region is not a sharp one, but extends over an energy range of at least an order of magnitude, as shown by the recent experiments of Bergström *et al.* (see Ref. 21).

[21] I. Bergström, K. Björkqvist, B. Domeij, G. Fladda, and S. Andersen, Can. J. Phys. **46**, 2679 (1968).

[22] These values have been obtained from the wave function calculations given in T. Hermann and S. Skillman, *Atomic Structure Calculations* (Prentice-Hall, Inc., Englewood Cliffs, N. J., 1963).

90% of the detected x rays originate were 6700 Å and 11 000 Å for GaP, and 3600 Å and 9400 Å for GaSb. One of the disadvantages of using x-ray measurements at these energies is that the mean depths are significantly greater than the minimum depth ($\approx$500 Å) that can be probed by backscattering. However, since the backscattering measurements can be made as a function of depth, they can be used to evaluate the small correction factor required to convert all the observed $\psi_{1/2}$ values to the same mean depth.

The measured critical angles and the values corrected to a depth of 1100 Å are given in Table III. In the ⟨111⟩ direction in GaP, the critical angle for the P x rays agrees well with the $\psi_{1/2}$ value measured at corresponding depths for backscattering from Ga for the ⟨111⟩ axial rows (which contain both types of atoms); this agreement is to be expected, as each ⟨111⟩ row contains both types of atoms (Fig. 2). For the ⟨110⟩ directions, however, the individual Ga and P rows should each exhibit their own critical angles at distances sufficiently close to the surface. The experimental $\psi_{1/2}$ value for the phosphorous x ray is clearly smaller than that obtained from the Ga backscattering yield (Table III). However, the magnitude of the effect $[(\psi_{1/2})_{Ga}/(\psi_{1/2})_P \approx 1.25]$ is somewhat smaller than that predicted by Eq. 2 $[(Z_{Ga}/Z_P)^{1/2}=1.44]$; this is attributed to the greater depths probed by the x rays which leads to some mixing of the effects from the two sublattices.

The Ga x-ray data are harder to interpret. In all cases where direct comparison can be made with the scattering data—viz., for the ⟨110⟩ and ⟨111⟩ directions in GaP and for the ⟨111⟩ direction in GaSb—the critical angles for the Ga x ray are ~12% lower than the backscattering values at comparable depths. This difference is probably due to the fact that the Ga L x-ray production has a finite cross section at impact parameters comparable to r_{min}, and hence does not fall to zero as the beam becomes channeled. In a more clear cut case (M-shell x rays in tungsten), Davies *et al.*[16] also found a significant reduction in the critical angle for M-shell x rays compared to the value for backscattering and for the inner (K and L) shell x rays. Because of this discrepancy, we cannot make a quantitative comparison between the $\psi_{1/2}$ values for the individual Ga and Sb rows along the ⟨111⟩ in GaSb. However, even after applying a 12% correction to the Ga data in Table III, it is evident that $(\psi_{1/2})_{Ga}$ is still considerably smaller than $(\psi_{1/2})_{Sb}$—as one would predict from the dependence in Eq. 2. However, as in the GaP case discussed above, this difference is not as large as the predicted value of 28%.

C. Planar $\psi_{1/2}$ Values

The comparison of critical angles for three different planes in silicon is shown in Fig. 10. By use of {110} oriented crystals and rotations through these planes at 14° from the ⟨110⟩, it was possible to obtain $(\psi_{1/2})_{planar}$ with an accuracy of $\pm 0.03°$. The individual planar

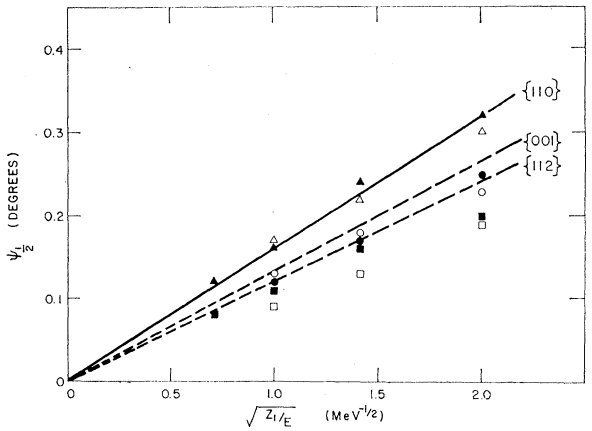

FIG. 10. Critical angles for several low-index planes in silicon plotted as a function of $\sqrt{(Z_1/E)}$: (110) data—▲ (H^+), △ (He^+); (001) data—● (H^+), ○ (He^+); (112) data—■ (H^+), □ (He^+). The solid line is the "best fit" to the (110) data; the dotted lines are the values calculated for the other planes from the (110) curve on the basis of a $(d_p)^{1/2}$ dependence.

critical angles increase linearly with $(Z_1/E)^{1/2}$, indicating that the predicted functional dependence on atomic number and energy of the projectile is correct. However, the variation of critical angle with lattice spacing (d_p) is much greater than predicted by Eq. (4), as can be seen by comparing the experimental data for the (001) and (112) planes (Fig. 10) with the solid curves predicted [Eq. (4)] from the best fit to the (110) plane. A similar discrepancy for these higher-order planes has also been observed in other studies.[8] Further investigations are underway to determine if more detailed calculations (similar to those carried out by Andersen[17]) will lead to better agreement. Note that any contribution from beam divergence or mosaic spread in the crystal tends to *reduce* the observed differences be-

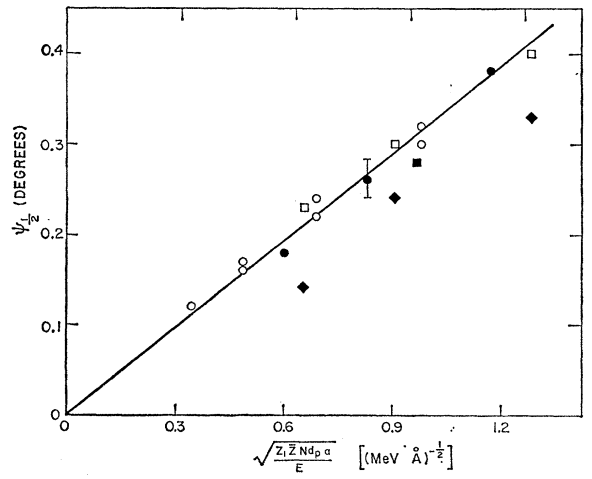

FIG. 11. Observed functional dependence of $\psi_{1/2}$ for the (110) plane in various semiconductor lattices: ○—Si; □—Ge; ●—GaP; ◆—GaAs; ■—GaSb.

tween the various planes and so would not explain the discrepancy.

Critical angles for the {110} plane in the various crystals are plotted in Fig. 11—with the functional dependence of lattice, projectile, and projectile energy incorporated into the abscissa on the basis of the average potential theory. The planar spacing d_p is 2.0 ∓ 0.1 Å for all the crystals considered—except diamond.[23] The experimental values of $\psi_{1/2}$ for all the lattices can be fitted reasonably well to a single relationship, indicating that apart from the lattice spacing (discussed above), the predicted functional dependence is obeyed. The slope gives a value of $\beta\approx1.5$.

In the comparison of the data in Fig. 11, no correction has been made for the variation of thermal vibrational amplitude in the different diamond lattices—unlike the axial channeling case in Fig. 9(b). For planar channeling, vibrational effects are generally not significant—presumably because the average planar potential varies much more slowly with impact parameter in the region of a than does the average row potential.[24] This difference between planar and axial channeling has previously been observed also as a marked difference in "dechanneling" rate as a function of temperature (i.e., of vibrational amplitude); in the axial case, the dechanneling rate is strongly temperature-dependent, but in the planar case, it is almost independent of temperature.[8]

The case of a mixed plane has also been investigated. The (110) plane was selected since the interplanar spacing is uniform and each plane contains equal numbers of the two atomic species. Thus, a single planar critical angle, based on the averaged potential, should be obtained. Experimental values of $\psi_{1/2}$ are compared with the monatomic results for the (110) plane in Fig. 11, using the averaged atomic number $\bar{Z}=\frac{1}{2}(Z_A+Z_B)$. The agreement is quite good for GaP and GaSb. However, the GaAs values are somewhat low; the reason for this discrepancy is not understood.

D. $\chi_{\min}$ Values

The minimum yield $\chi_{\min}$ [$\chi_{\min}$=(aligned yield)/(random yield)] near the surface is another useful experimental parameter for characterizing the channeling behavior. An estimate of the minimum yield for axial channeling can be expressed by[11]

$$\chi_{\min}=\pi N d r_{\min}^2, \tag{5}$$

where N is the atomic density, d the spacing along the row, and $r_{\min}$ is the closest distance of approach between a channeled beam and an aligned row. Rough estimates for $\chi_{\min}$ can be obtained: (i) for a nonvibrating lattice, by setting $r_{\min}\simeq a$ (the Thomas-Fermi screening distance) and (ii) for a lattice in which the mean-square vibrational amplitude $\langle\rho_r^2\rangle_{\rm av}$ (measured perpendicular to the row) is large, by setting $r_{\min}^2\simeq\langle\rho_r^2\rangle_{\rm av}$. However, a better procedure[25] is to use an approximate relationship between $\psi_{1/2}$ and $r_{\min}$,

$$E(\psi_{1/2})^2=U(r_{\min}), \tag{6}$$

where the average potential is given by

$$U(r_{\min})\approx(Z_1Z_2e^2/d)(\pi a/2r_{\min}).$$

Together with Eq. (5), this gives

$$\chi_{\min}=\pi N d(\tfrac{1}{4}\pi a)^2(\psi_1/\psi_{1/2})^4, \tag{7}$$

and enables the contribution from thermal vibrations to be expressed in terms of the experimentally determined ratio of $\psi_{1/2}$ to ψ_1.

Measured and estimated values of $\chi_{\min}$ are compared in Table II. For the cases of Si, Ge, GaP, and diamond, the observed values of $\chi_{\min}$ agree reasonably well with the values given by Eq. (7). In the other crystals studied here (GaSb and GaAs), the $\chi_{\min}$ values are considerably larger than predicted. It should be pointed out that surface contamination, lattice defects, etc., always tend to increase the observed value of $\chi_{\min}$. This may perhaps explain why these two crystals (GaAs and GaSb) exhibit values of $\chi_{\min}$ significantly larger than those given by Eq. (7).

In all cases, the observed values of $\chi_{\min}$ are considerably greater than the estimated lower limit of $Nd\pi\langle\rho_r^2\rangle_{\rm av}$ (Table II), set by thermal vibrations alone.

V. SUMMARY

We have investigated proton and helium channeling in diamond-type lattices, and have measured $\psi_{1/2}$ and $\chi_{\min}$ values *near the surface* for comparison with theory, since the existing treatment does not yet account quantitatively for depth effects. The high-energy region ($\psi_{1/2}\lesssim a/d$) has been studied over a wide range of lattice parameters.

The axial critical angles have a functional dependence which agrees well with average potential calculations, using appropriate values for the thermal vibrational amplitude of the lattice atoms. This agreement extends both to uniform and nonuniform atomic spacing and to monatomic and diatomic rows of atoms. For those directions along which the different atomic species lie on separate rows (i.e., ⟨110⟩), the data indicate that each row steers the incident particles in a manner described by the average potential of that row. For *axial* channeling, the measured values of the critical angle are approximately 25% lower than the calculated ones. The reason for this discrepancy is not known.

The theory as discussed in Sec. III explains also the functional dependence for *planar* channeling—except with respect to the interplanar spacing. The measured

[23] Diamond has a considerably smaller value of d_p (viz., 1.3 Å), and has therefore been omitted from this intercomparison.

[24] For calculated "average potentials," see, for example, Refs. 11 and 12.

[25] We are indebted to J. U. Andersen and L. Feldman for suggesting this derivation of $\chi_{\min}$ in terms of $(\psi_1/\psi_{1/2})$.

values of $\psi_{1/2}$ for planar channeling decrease much more rapidly with decreasing planar spacing than predicted by Eq. (4).

The observed values of the axial minimum yield (a measure of the unchanneled fraction of the beam) agree well with the theoretical estimates in the case of C (diamond), Si, Ge, and GaP lattices. In GaAs and GaSb, however, the observed values are significantly larger than expected; this is attributed to the influence of oxide layers, surface contamination or lattice imperfections.

Note added in proof: More detailed calculations which include the effect of surface transmission show agreement with the experimentally observed $\psi_{1/2}$ dependence on planar spacing. Results to be published by S. T. Picraux and J. U. Andersen.

ACKNOWLEDGMENTS

We are indebted to Dr. F. Trumbore for supplying the GaP samples, and to Dr. J. McNeely for the GaAs and GaSb samples. We particularly want to thank Ian Mitchell for his participation in the x-ray measurements and in their subsequent interpretation. The assistance of G. R. Bellavance and G. A. Sims with the Van de Graaff bombardments and of P. Kjær with the 50-keV H^+ measurements is also gratefully acknowledged.

PHYSICAL REVIEW VOLUME 180, NUMBER 3 15 APRIL 1969

Impurities and Secondary Reactions in Radiation Defect Production at Liquid-Nitrogen Temperature in Alkali Halides*

E. SONDER,† G. BASSIGNANI, AND P. CAMAGNI
Solid State Physics, Centro Comune Ricerche Nucleari Euratom, Ispra, Italy
(Received 11 December 1968)

The F-center production rate due to electron irradiation at 80°K has been measured in pure KCl and KBr, in KCl doped with Ag, Ca, Cd, Co, and Tl, and in KBr doped with Ca and Cl. In every case an enhancement of the defect production rate was observed in samples containing between 1 and 100 ppm impurity. Accompanying the enhancement of the F-center production rate was a saturating growth of ultraviolet absorption, usually in the V_1 region of the spectrum, and a temporary suppression of the growth of the intrinsic ultraviolet absorption band (240 nm for KCl and 275 nm for KBr, sometimes labeled V_4). In KCl samples containing more than 100 ppm impurity, the 240-nm band was observed to shift to shorter wavelengths. In addition, the stability of the defects produced in doped samples was found to be less upon warming or bleaching than that of pure samples. The F-center growth curves have been compared with predictions of a model in which free interstitials can either recombine with vacancies or be trapped by defects. The curve shapes suggest that the model in its simplest form is not valid, and that perhaps most of the interstitials and vacancies remain correlated.

I. INTRODUCTION

IN a recent study[1] of color center production at liquid-nitrogen temperature it was found that lead impurity could significantly enhance the rate of F-center formation. It was suggested in that work that the lead acted as a trap for mobile interstitial defects and thus enhanced the colorability by impeding the recombination of defects.

Whether the complicated radiation damage behavior of alkali halides at temperatures above the liquid-helium range is due to a number of different production processes or is simply due to recombination and other secondary reactions following one efficient primary production mechanism[2] is a rather basic question.[3] For this reason we felt that a more extended study of the influence of impurities on defect production at liquid-nitrogen temperature would be useful. In particular, we wanted to test the suggestion that interstitial trapping impedes recombination of interstitials and vacancies. Therefore, we decided to irradiate at liquid-nitrogen temperature, where interstitials in KCl are mobile, and to see whether the enhancement of defect production that had been observed for lead doping[1] could also be found in KCl doped with impurities of different valence and size. We present here results of investigating KCl(Ag) rather extensively and KCl(Ca), KCl(Tl), KCl(Co), and KCl(Cd) in a more rudimentary fashion. We also report a few results obtained with doped KBr.

* Work supported in part by the U. S. Atomic Energy Commission.

† Guest scientist from Solid State Division, Oak Ridge National Laboratory, Oak Ridge, Tenn.

[1] E. Sonder and W. A. Sibley, Phys. Rev. **140**, A539 (1965).

[2] D. Pooley, Proc. Phys. Soc. (London) **87**, 245 (1966); H. N. Hersh, Phys. Rev. **148**, 928 (1966).

[3] For a review of the history and recent work connected with this problem, see J. H. Crawford, Jr., Advan. Phys. **17**, 93 (1968); see also Refs. 1, 14, 15, and J. H. Crawford, Jr., W. A. Sibley, and E. Sonder, Phys. Status Solidi **23**, 301 (1967).